A Multi-Sensorization Approach to Improve Safety in Transesophageal Echocardiography

Giovanni Faoro, *Graduate Student Member, IEEE*, Izadyar Tamadon, Selene Tognarelli, and Arianna Menciassi, *Fellow, IEEE*

***Abstract*—Real-time 3D transesophageal echocardiography (RT-3D TEE) allows 3D visualization of patient heart and catheters without exposing patient and operators to ionizing radiations. Nonetheless, during such procedures esophageal injuries occur due to improper probe manipulation and probe overheating. To tackle these problems, we propose a multisensorization approach to provide information on probe pose and temperature throughout the procedure. Electromagnetic (EM) tracking is fused with inertial sensing thanks to a finite state machine integrating Extended and Incremental Kalman filters. This approach allows for a statistically significant improvement in static tracking with respect to standard EM, as reported by the Mann-Withney test. A novel sensor fault detection based on angular velocities discrepancy allows for robust tracking under different electromagnetic interferences, such as the one provided by ferro-, dia- and paramagnetic materials occupying the interventional room. Fiber optic technology is exploited for temperature estimation, taking advantage of its immunity to EM fields and the possibility of distributed sensing. Performances are compared with a commercial thermistor to guarantee feasibility and a root mean square error of 1.59 °C is finally reported. We believe that these results demonstrate how sensing technologies can be integrated in TEE-guided surgical procedures to improve overall outcome and safety.**

***Index Terms*—Sensor fusion, electromagnetic tracking, inertial sensors, transesophageal echocardiography, temperature estimation.**

I. Introduction

MINIMALLY invasive transcatheter cardiovascular intervention has been adopted in the late 90s to replace, whenever possible, open-heart procedures. It enables faster recovery and reduces pain compared with complete or partial sternotomy [1]. The recent development of real-time 3D transesophageal echocardiography (RT-3D TEE) enabled the execution of several trans-catheter interventions under real-time image guidance [2], [3]. However, recent studies highlighted the occurrence of esophageal injuries after cardiac surgery under TEE guidance. Blind probe insertion, advancement of improperly placed probe and continuous adjustment for optimal instrument guidance, together with heating of the device and of the tissue from prolonged use, seem to be the main causes of problems [4], [5].

Improper manipulation can cause mechanical trauma to the esophagus due to excessive forces exerted on the tissue or improper positioning of the tip with respect to the patient specific anatomy. The esophageal injuries deriving from these factors can range from minor lesions, like petechiae and ecchymosis, to more serious lesions, like intramural hematoma or mucosal laceration [5]. Information on tip position can help in improving procedure safety under several aspects. It enables registration with pre-operative data and volume compounding. The former is used to provide a guidance thanks to pre-operative diagnostic images, while the latter allows an increase in the field-of-view (FoV). Additionally, after proper calibration, the knowledge on the ultrasound (US) probe tip position allows to associate spatial information to image pixels and thus infer the spatial pose of the imaged intracardiac catheter. These steps can increase procedure safety by providing precise instructions to either the human operator or a robotic arm on how to manipulate the TEE probe and the intracardiac catheter in order to optimally follow the specific patient anatomy. When dealing with endoscopic devices, as the TEE, the unavailability of free line-of-sight hampers the use of gold-standard optical tracking, setting the need for alternative strategies such as electromagnetic (EM) tracking [6]. Anyway, EM tracking of surgical instruments can be compromised by magnetic field distortions generated by nearby medical diagnostic devices (as fluoroscopy arm), other ferromagnetic objects (as other surgical instruments) or even by the instrument itself. To address the effects of such disturbances in a standardized way, several platforms and protocols have been proposed [7], [8], [9]. While this is helpful in understanding EM tracking potentialities for a given application, studies reported a strong deterioration of sensor performances when moving from bench to bedside [10]. This suggests that EM sensors alone might be insufficient for intra-operative tracking, and more complex strategies should be considered, pushing forward the adoption of sensor fusion. In [11] an Extended Kalman Filter (EKF) was considered to fuse EM information with Inertial Measurement Unit (IMU) data to track an endoscopic device. A similar

Manuscript received 15 December 2023; revised 22 April 2024; accepted 5 May 2024. Date of publication 30 May 2024; date of current version 5 August 2024. This article was recommended for publication by Associate Editor P. Fiorini and Editor P. Dario upon evaluation of the reviewers' comments. This work was supported by the European Union's Horizon 2020 Research and Innovation Programme through the ARTERY Project under Grant 101017140. *(Corresponding author: Giovanni Faoro.)*

Giovanni Faoro, Selene Tognarelli, and Arianna Menciassi are with the BioRobotics Institute and the Department of Excellence in Robotics and AI, Scuola Superiore Sant'Anna, 56127 Pisa, Italy (e-mail: giovanni.faoro@santannapisa.it; selene.tognarelli@santannapisa.it; arianna.menciassi@santannapisa.it).

Izadyar Tamadon is with the Faculty of Engineering Technology, University of Twente, 7522 NB Enschede, The Netherlands, and also with the BioRobotics Institute, Scuola Superiore Sant'Anna, 56025 Pontedera, Italy (e-mail: i.tamadon@utwente.nl).

Digital Object Identifier 10.1109/TMRB.2024.3407378

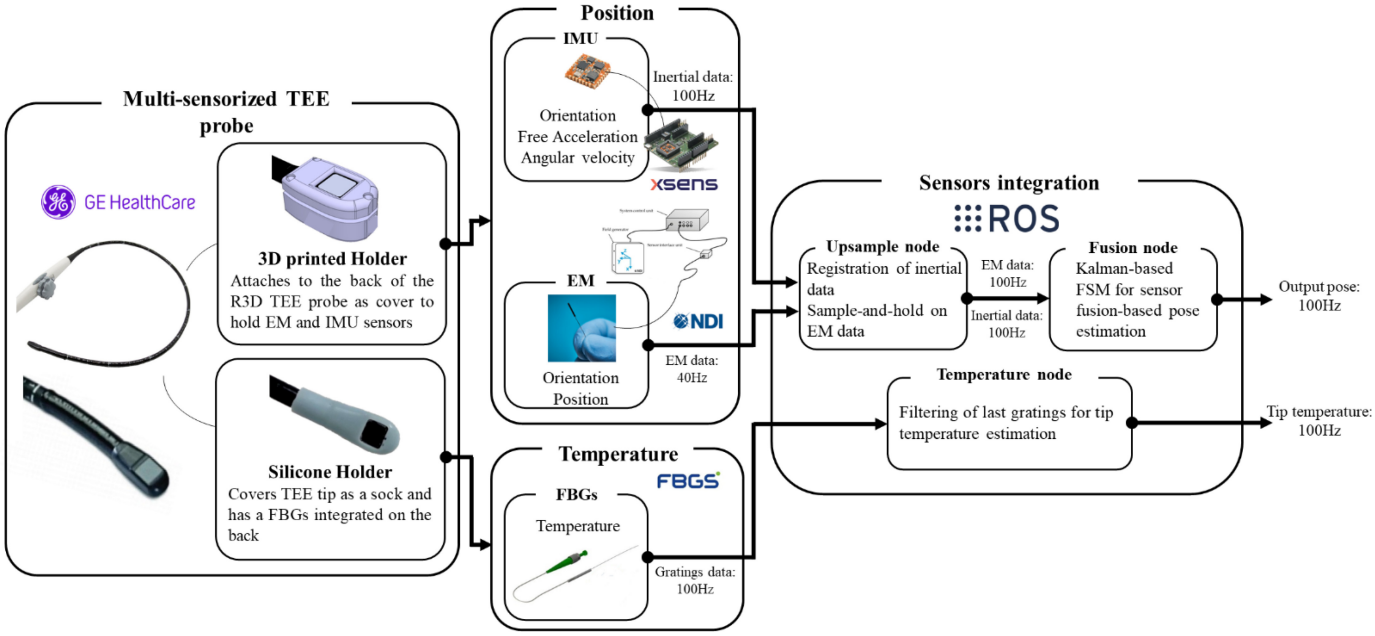

Fig. 1. Sensor fusion and integration schematic. Two different sensor holders are considered for position and temperature estimation. The former is a rigid 3D printed structure so to maintain the relative position of EM and IMU fixed throughout the procedure. The latter is a silicon cuff embedding a FBGs fiber on its back. Data are acquired with sensor specific software but all streamed and analyzed in a single ROS network (to ease future robotization) achieving high update rates.

approach was investigated in [12] to track the tip of a catheter which should anchor to an organ for its motion estimation. Kalman filters were also used to estimate the position of a needle tip fusing multiple EM sensors data with kinematic needle deflection model [13]. Multiple EM data were merged with magnetic distortion maps through a combination of EKF and Simultaneous Localization and Mapping (SLAM) techniques for transrectal US probe and transbronchial needle tracking [14], [15]. Despite this interest toward sensor fusion to improve endoscopic and endoluminal device detection, TEE tracking was most of the time addressed with standard EM sensors [16], [17], [18], [19], [20]. Probe tip position data were considered to register with other imaging techniques [16], to increase FoV [17], to improve instrument navigation [20] or for robotic manipulation [21], [22], [23]. In this specific scenario, also a custom sensing approach based on permanent magnets was investigated [24].

The endoluminal nature of the TEE probe also brings out a peculiar issue, not evident in other US devices, as overheating due to Joule effect, dissipating heat to surrounding tissues. In vitro and in vivo studies observed that cell death is triggered by a thermal dose, which can be defined as exposure to a given temperature for a certain time. It has been reported that cells can withstand exposure to 41°C for more than 10 hours but just for 1 minute to 43°C [25]. Standard TEE-guided operations, as edge-to-edge mitral valve procedures, can last for more than 2 hours thus exposing the patient to thermal risk if TEE probe temperature is not correctly handled [4]. Currently, probe overheating is not fully addressed by commercial devices. Only few models are provided with internal sensors and automatically shut down when temperature exceeds a given threshold. For example, TEE Philips user manual reports the integration of one internal thermistor to get an alert message at 41°C with an automatic shutdown at 42.5°C [26]. Similar indications can be found also for GE Healthcare [27]. Anyhow, during an image-guided procedure, automatically shutting down the TEE probe means losing any US-related information on patient anatomy and intracardiac catheter position. To continue the procedure, surgeons need to rely solely on the use of fluoroscopy, which is commonly used only occasionally to help checking for proper positioning. The shutdown, that is risky per se, exposes patient, surgeons and sonographers to an increased uptake of ionizing radiations and thus an increased oncological risk [28]. In this scenario, a continuous temperature monitoring could improve procedure safety by enhancing operator awareness on the probe temperature, in order to plan in advance possible correction actions, or by enabling automatic cooling devices.

Within this context, and following the schema reported in Fig. 1, in this paper we address TEE probe multi-sensorization with two objectives: (i) to stably detect TEE probe position regardless of external disturbances and (ii) to continuously monitor probe temperature. To achieve the former point, sensor fusion strategies are considered to take advantage of two independent information sources, such as EM and IMU sensors. Major focus is placed on static probe tracking as this is the condition when the TEE probe is placed in the esophagus acquiring images of the heart and manipulation of other devices in the surrounding environment occurs (e.g., insertion of the intracardiac catheter). In this scenario, TEE probe position detection is fundamental to carry out volume compounding with small tip motion or infer intracardiac catheter position with respect to surrounding anatomy thanks to real-time US imaging. During TEE probe insertion in the

esophagus very little sensor interferences are expected as the sonographer still needs to properly position the probe and thus no other devices are manipulated nearby. The second objective is addressed by considering optical fiber temperature sensing. Optical fibers have been investigated for several purposes as shape [29], force [30] and temperature sensing [31] in view of multiple advantages of fibers, as miniaturization, chemical inertness and immunity to electromagnetic fields. The latter property is fundamental to avoid mutual disturbances of fiber-based temperature estimation with position tracking.

The major contributions to advancements in TEE probe sensorization presented in this paper are the following: 1) standardized assessment of EM sensor performances for TEE probe through the Hummel's protocol [8]; 2) presentation of a novel global-local registration routine between EM and IMU based on angular velocities as a generalization of Chardonnens' algorithm [32]; 3) a novel finite state machine for sensor fusion based on the integration of EKF with Incremental Kalman Filter (IKF) with angular velocities-based sensor fault detection; 4) comparison of Fiber Bragg Grating sensor (FBGs) with a thermistor for biomedical applications. Additionally, all these sensing strategies were developed in or bridged to the Robot Operating System (ROS) to ease future integration in robotic platforms. Last, pose and temperature estimation were considered separately for setup simplification, as optical fibers immunity to electromagnetic fields does not alter electromagnetic sensors performances and viceversa.

The remainder of this article is organized as follows: Section II describes the hardware components and the software framework. Section III is dedicated to the EM-IMU registration and sensor fusion, whereas Section IV presents the comparison between thermistor and FBGs. Section V reports and discusses experimental results and Section VI remarks on the conclusions and the future perspectives stemming from this article.

II. Hardware and Software Components

In this section the details on the experimental setup, in terms of hardware and software components, are reported including: (i) the selected TEE probe, sensors, design and fabrication of sensor holders and platforms for validation; (iii) software integration.

A. Hardware: TEE Probe, Sensors and Holders

In this study, the RT-3D TEE probe manufactured by GE is considered as the device to be sensorised (6VT-D, GE Healthcare, Chicago, Illinois, USA). An Aurora Micro 6DOF Sensor (Northern Digital, Inc., Waterloo, Ontario, Canada) with a Planar Field Generator (PFG) is selected as EM sensor to track TEE tip position and orientation. To assess sensor performances in a standardized way, the Hummel's protocol is considered [8]. The validation platform consists of a main Plexiglass plate with a 4x4 grid of holes spaced 50 mm apart and dedicated to position measurements. The grid has been obtained by laser cutting machining (VLS4.75, Universal laser systems). In the center, a circular pattern of 32 holes in radius of 50 mm and spaced 11.25° apart from each other is

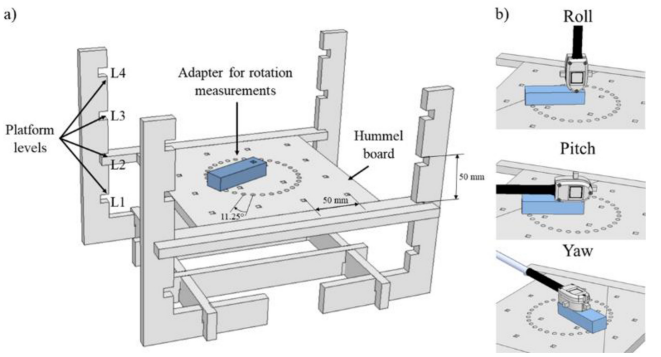

Fig. 2. Design of the experimental platform for the assessment of EM performances through Hummel's protocol. In panel a) plate for grid measurements (Hummel board), adapter for rotation measurements and multilevel structure are shown. Panel b) depicts the probe configuration for rotations along the tree different axes (i.e., roll, pitch and yaw).

exploited for accurate measurements of rotations. In addition, a Plexiglass structure has been designed to place the main plate at 4 different levels (L1-4) spaced by 50 mm (see Fig. 2a). To firmly attach the EM sensor to the probe tip allowing also the connection to the assessment board, a custom-made holder is 3D printed (Prusa i3 MK3S+). It is characterized by a site aligned with shaft long axis for EM sensor placement on the back surface of the probe tip and cubic pillars along three orthogonal axes to investigate tracking performances during roll, pitch and yaw rotations (see Fig. 2b). The holder also allows the integration of an inertial sensor for measuring the device pose (MTi-7-DK, Xsens Technologies, Enschede, The Netherlands) on the backside of the probe. The two sensors are placed close together on the small back surface of the probe tip, which is 41 mm in height and 16 mm in length.

Last, an FBG sensor (FBGS International NV, PR2022 14 62 06S03) is tested along with a thermistor (Amphenol, Thermistor NTC. MC65F502BN) with the purpose to compare their performances on temperature estimation. The FBG was connected to the interrogator (FBGS-scan 904), a specialized hardware that generates the optical source and provides the optical fiber feedback accessible via ILLumiSense (v3.1.23) program. To secure the fiber in place on the back of the probe, a silicone cuff of 2 mm thickness was created (Smooth-on, Smooth-Sil 936). This allows also to evaluate different sensors-probe integration approaches.

B. Software Integration

Recent studies highlighted the potential of robotic US to improve and standardize image acquisition for both extra-corporeal and TEE probes [33]. To ease future integration of the presented sensing strategies with robotic control (e.g., automatic and motorized insertion and navigation of catheters), a ROS network managing data acquisition and elaboration is developed. The IMU of Xsens already provides inertial data at 100 Hz to a ROS topic when connected to its own electronic board. EM sensors data are streamed at 40 Hz to a ROS topic thanks to the use of OROCOS middleware. On the other hand, FBGs data can only be acquired with the ILLumiSense program that is not available for Ubuntu operating systems.

This constraint makes necessary the use of two different computers with custom communication and ROS integration. Thus, FBGs data are streamed locally on a Windows computer thanks to ILLumiSense. A Python (v2.7.18) script is used to republish them over the Internet on a Mosquitto message broker (v1.6.9) using the MQTTv3.1.1 protocol. A bridge node on the Ubuntu computer subscribes to the broker topic and converts MQTT messages into ROS messages publishing them at 100 Hz to the ROS network.

The ROS network is able to collect data from the three different sensors and process them through dedicated nodes. Temperature estimates are retrieved by simply averaging measurements of the last two gratings. Pose information is instead computed considering EM data upsampling via sample and hold strategy (to let them reach 100 Hz as IMU data), EM-IMU registration and fusion, which are detailed in the next sections.

III. Finite State Machine Kalman-Based Sensor Fusion for EM and IMU Sensors

The Kalman filter is an iterative algorithm exploiting a statistical approach to provide estimates of unknown variables. It is based on a prediction step, in which new variables values are foreseen based on a physical model describing the observed system, and on an update step, where sensor measurements are used to refine variable values [34].

Throughout this article, the following nomenclature is considered. Scalars are denoted by lowercase fonts (e.g., ω_x), vectors by bold lowercase fonts (e.g., $\boldsymbol{\omega}$) and matrices by bold uppercase fonts (e.g., $\mathbf{K}$). The rotation matrix from reference frame A to B is indicated as $\mathbf{R}_B^A$, the nxn identity matrix is specified by $\mathbf{I_n}$, * indicates the complex conjugate and $\times$ indicates the quaternion product. Last, when dealing with the Kalman filter, $\mathbf{x}_{k+1k}$ indicates the prediction of $\mathbf{x}$ at step k + 1 based on its value at step k, while $\mathbf{x}_{k+1|k+1}$ indicates the update of $\mathbf{x}$ at step k+1 based on its prediction at step k + 1.

In the next subsections, details on the novel approaches for sensor data registration and fusion are provided.

A. Sensors Registration

One of the main applications of Kalman filters is to combine data from different sources to improve the final estimate. Anyway, since every sensor is providing data in its own local or global reference frame, a fundamental step before sensor fusion is registration. It allows to align sensor reference frames and thus makes information coherent between them. There are several methods tackling registration based on the well-known hand-eye calibration problem. Anyway, most of them consider Paired-Point Alignment (PPA) requiring as input a set of 3D points acquired by the two different measuring systems. Instead, when dealing with inertial sensors we need to consider Paired-Orientation Alignment (POA), which just requires 3D orientations (the only common information between IMU and EM) and output rotation rather than transformation matrices [35]. An example of POA is the Chardonnens' method, which allows to compute the rotation matrix between local reference frames of two relatively fixed sensors from local angular velocities $\boldsymbol{\omega}$ [32]. Since the two sensors are relatively fixed and attached to the moving target, the measured angular velocities should just differ by the initial misalignment of the two reference frames. This assumption is correct also in the global systems, as IMU global reference frame is the East-North-Up (ENU) world reference frame and the EM global reference frame is fixed to the PFG. Thus, given the real-time availability of the rotation matrices $\mathrm{R}_{\mathrm{Coil}}^{\mathrm{Aurora}}$ (from PFG to EM sensor, as in Fig. 3) and $\mathbf{R}_{\mathrm{IMU}}^{\mathrm{ENU}}$ (from ENU to IMU) in forms of quaternion, we would like to estimate the constant rotation matrices $\mathbf{R}_{\mathrm{Coil}}^{\mathrm{IMU}}$ and $\mathbf{R}_{\mathrm{ENU}}^{\mathrm{Aurora}}$, between local and global frames respectively. These can be computed by extending the Chardonnens' method also to global frame registration, as the underlying assumptions still hold, if global angular velocities Ω are available. Both local and global angular velocities can be easily retrieved exploiting quaternions $\mathbf{q}$, as reported in eq. 1-2

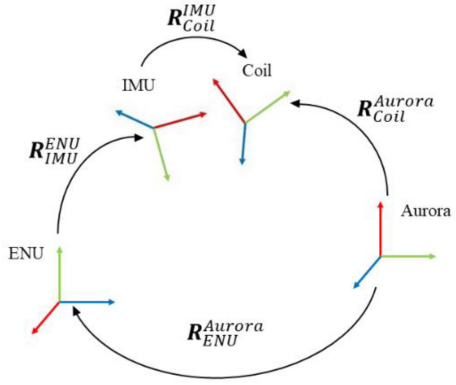

Fig. 3. Rotation matrices between local and global reference frames. The EM sensor is providing the rotation matrix $\mathrm{R}_{\mathrm{Coil}}^{\mathrm{Aurora}}$, while $\mathbf{R}_{\mathrm{IMU}}^{\mathrm{ENU}}$ is given by IMU data. The goal of the registration routine is to compute the local rotation matrix $\mathbf{R}_{\mathrm{Coil}}^{\mathrm{IMU}}$ and the global one $\mathbf{R}_{\mathrm{ENU}}^{\mathrm{Aurora}}$.

$$\boldsymbol{\omega} = \lim_{dt\to 0} 2Im\left(\frac{\mathbf{q}^*(t)\times\mathbf{q}(t+dt)}{\mathrm{dt}}\right) \tag{1}$$

$$\boldsymbol{\Omega} = \lim_{dt\to 0} 2Im\left(\frac{\mathbf{q}(t+dt)\times\mathbf{q}^*(t)}{\mathrm{dt}}\right) \tag{2}$$

where Im denotes the imaginary part of the complex quaternion product, which is not commutative.

B. Sensor Fusion

To exploit the general Kalman filter theory described in eq. (1)–(8) it is necessary to define a state vector $\mathbf{x}$, a measurement vector $\mathbf{z}$ and the measurement and model equations f and h. In our case study, the state vector is $\mathbf{x}_k = [\mathbf{q}, \boldsymbol{\omega}, \mathbf{p}, \mathbf{v}, \mathbf{a}]$ representing TEE probe tip orientation, angular velocity, position, velocity and acceleration, respectively. The measurement vector $\mathbf{z}_k$ is instead defined as $[\mathbf{q_{EM}}, \mathbf{p_{EM}}, \mathbf{q_{IMU}}, \boldsymbol{\omega}_{\mathbf{IMU}}, \mathbf{a_{IMU}}]$, where subscripts indicate the information source. The formulation of the state transition function f is reported in (3)–(8).

$$\mathbf{q}_{k+1|k} = \left(\cos\left(\frac{\|\boldsymbol{\omega}_{k|k}\|\mathrm{dt}}{2}\right)\mathbf{I}_4 + \frac{\sin\left(\frac{\|\boldsymbol{\omega}_{k|k}\|\mathrm{dt}}{2}\right)}{\|\boldsymbol{\omega}_{k|k}\|}\mathbf{L}(\boldsymbol{\omega}_{k|k})\right)\mathbf{q}_{k|k} \tag{3}$$

where $\mathbf{L}$ is given by [36]

$$\mathbf{L}(\boldsymbol{\omega}) = \begin{bmatrix} 0 & \boldsymbol{\omega}_z & -\boldsymbol{\omega}_y & \boldsymbol{\omega}_x \\ -\boldsymbol{\omega}_z & 0 & \boldsymbol{\omega}_x & \boldsymbol{\omega}_y \\ \boldsymbol{\omega}_y & -\boldsymbol{\omega}_x & 0 & \boldsymbol{\omega}_z \\ -\boldsymbol{\omega}_x & -\boldsymbol{\omega}_y & -\boldsymbol{\omega}_z & 0 \end{bmatrix} \tag{4}$$

$$\boldsymbol{\omega}_{k+1|k} = \mathbf{I}_3 \boldsymbol{\omega}_{k|k} \tag{5}$$

$$\mathbf{p}_{k+1|k} = \mathbf{p}_{k|k} + dt\mathbf{I}_3 \mathbf{v}_{k|k} + \frac{\mathrm{dt}^2}{2}\mathbf{I}_3 \mathbf{a}_{k|k} \tag{6}$$

$$\mathbf{v}_{k+1|k} = \mathbf{v}_{k|k} + dt\mathbf{I}_3 \mathbf{a}_{k|k} \tag{7}$$

$$\mathbf{a}_{k+1|k} = \mathbf{I}_3 \mathbf{a}_{k|k} \tag{8}$$

Equations (5) and (8) might be interpreted as assumptions of constant rotation velocity and linear acceleration for the body to be tracked. This is done to exploit the Kalman filter for low-pass filtering raw sensor data and thus removing high-frequency noise. From eq. (3) it is also clear how the developed filter is not linear in the state evolution, thus motivating the adoption of the EKF formulation. On the other hand, the formulation of the measurement model h is linear in the state and provided in eq. (9).

$$\mathbf{z}_{k+1|k} = \begin{bmatrix} \mathbf{I}_4 & 0 & 0 & 0 & 0 \\ 0 & 0 & \mathbf{I}_3 & 0 & 0 \\ \mathbf{I}_4 & 0 & 0 & 0 & 0 \\ 0 & \mathbf{I}_3 & 0 & 0 & 0 \\ 0 & 0 & 0 & 0 & \mathbf{I}_3 \end{bmatrix} x_{k+1|k} \tag{9}$$

The model covariance matrix $\mathbf{P}$ is initialized as a diagonal matrix with values equal to 0.0001 reflecting the assumption of knowing the initial state with a small variance. The model error covariance matrix $\mathbf{Q}$ is defined as a diagonal matrix with values equal to 0.00003, taking inspiration from [12]. This basically states that we are describing the physics of the phenomena under observation in a precise and confident way. Finally, the measurement error covariance matrix $\mathbf{R}$ is initialized by sensor performances reported in the datasheets and updated at each iteration thanks to the variance propagation rule, since in the measurement vector we are considering also indirect sensor measurements as $\mathbf{q}_{\mathbf{IMU}}$. Last, it is possible to exploit both Extended and Incremental Kalman Filter (IKF) formulations with a finite state machine. This approach is grounded on the experimental observation that the EM sensor data are reliable in absolute value only when working in a controlled environment. When a magnetic perturbation occurs, we can distinguish between two different phases, a transient and steady-state phase. In the transient phase, sensor data are characterized by unpredictable oscillations and thus are completely unreliable. On the other hand, during the steady-state phase sensor data can be considered reliable only if computing the relative increment, since they are affected by a constant bias, and so IKF allows an improvement in performances [37]. For these reasons, we develop a finite state machine that manages to integrate EM and IMU sensor data differently based on the three possible scenarios:

- State 1. A magnetic perturbation never occurred. EM data can be considered as reliable and directly integrated with registered IMU data via an EKF.
- State 2. A sensor fault has been detected and we are in the transient perturbation phase. EM data are unreliable; thus, the output pose is solely based on IMU data integration.
- State 3. A sensor fault has been detected but we are in the steady-state perturbation phase. EM data are reliable if taken as incremental measurements, thus an IKF can be exploited.

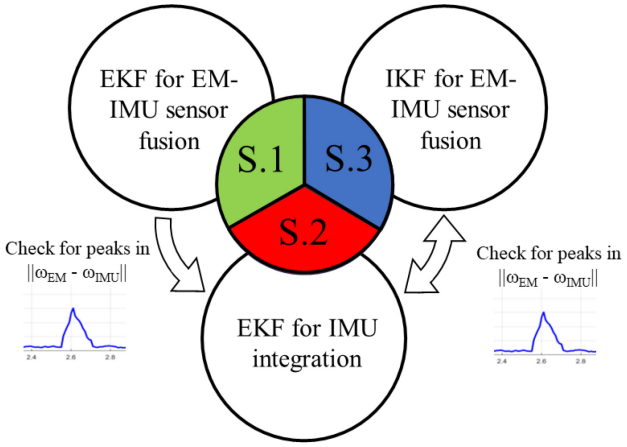

Fig. 4. Schematic representation of the proposed finite state machine. State 1 (S.1) corresponds to the unperturbed case, while State 2 (S.2) and State 3 (S.3) correspond to the transient and steady state of interference, respectively.

In State 3 the implemented filter cannot be exactly defined as a standard IKF since measurement increments $\mathbf{z}_{k+1|k+1} - \mathbf{z}_{k|k}$ are not directly used as inputs of filter update step. Indeed, measurement increments are exploited to adapt the last reliable measurement in order not to change the following integration equations.

Transition among states is determined by the value of a control variable defining goodness of EM data. Commonly, magnetometer data are exploited to detect EM sensor faults [12]. Anyway, this strategy is not sensitive to perturbations from diamagnetic or paramagnetic materials, such as copper or aluminum, respectively, but just to perturbations from ferromagnetic materials such as iron. A new control variable defined as the norm of angular velocities deviation between the one computed with IMU and EM data is proposed. Any perturbation will disturb EM sensor data causing deviations in sensor position and orientation estimates. The deviations on orientation will reflect in high instantaneous angular velocities, with no match on the IMU gyroscope data and generating easily detectable peaks in the control variable. An overview of the proposed finite state machine is reported in Fig. 4, which illustrates that it is not possible to go back to State 1: once EM sensors are perturbed, their measurements should be considered as incremental.

IV. FBGs for Temperature Estimation

Continuous and precise temperature estimation can be beneficial to improve TEE-guided procedures safety, by improving the way in which TEE overheating is currently handled (e.g., enabling the development of cooling systems). With respect to standard thermistors currently integrated in commercial devices, optical fiber-based sensing provides several advantages such as distributed sensing and higher update rates. To

investigate the reliability of FBGs (FBGS International NV, PR2022 14 62 06S03) temperature estimation, a comparison with a commercial thermistor (Amphenol, Thermistor NTC. MC65F502BN) is carried out. The two sensors are immersed in a water reservoir with different temperature excursions, controlled with a hot plate (IKA C-MAG HS7) equipped with its own thermocouple (IKA ETS-D5). In particular, a condition mimicking probe overheating is simulated. At first, a sudden change in temperature is produced from room temperature (around 22-25°C) to 37-38°C (resembling internal human body temperature). Secondly slow heating up to 50°C is produced to emulate probe overheating. Last, sudden change from 50°C to room temperature is used to simulate probe extraction. These conditions are deemed relevant for the specific application. These experiments are also carried out with FBGs free and integrated in the silicon shield to evaluate whether the silicon cuff will hamper precise temperature estimation.

V. Experimental Results

This section illustrates the evaluation of the sensorization strategies performances in terms of: (1) EM accuracy and precision in position and orientation estimation based on Hummel's protocol; (2) sensor registration performances; (3) stability and improvements of the sensor fusion estimate with respect to standard EM; (4) estimated temperature deviations between FBGs and thermistor.

A. Hummel's Board

Precision and accuracy are two standard metrics for sensor evaluation as they provide information on data dispersion and deviation from ground truth, respectively. When dealing with the Hummel's board, position accuracy, Acc_p, is computed as the absolute deviation between ground truth grid points distance (known by design), d_{gt}, and the measured Euclidean distance, d_i, between two locations, $\mathbf{p_i}$, where $d_i = \|\mathbf{p}_i - \mathbf{p}_{i+1}\|$; $\mathbf{p}_i = [(\sum_{j=1}^{\mathrm{Ns}} \mathbf{p}_{\mathrm{ij}})/(N_s)]$; $\mathbf{p}_i \in \mathbb{R}^3$; $i = 1, \ldots, N_L$ represents the number of locations and $j = 1, \ldots, N_s$ the number of samples. Three different ground truth distances can be computed, depending on the considered grid points, namely 50, 100 or 150 mm. The orientation accuracy, Acc_o, is similarly calculated considering the absolute difference between the ground truth rotation angle (known by design), α_{gt}, and the measured angle, α_i, between two pairs of rotations, $\mathbf{q_i}$. Since rotation measurements are collected in quaternion form, the peculiar math for this kind of information representation should be considered. Thus, the angle between two quaternions can be computed as: $\alpha_i = 2\cos^{-1}(\overline{\mathbf{q}}_i \overline{\mathbf{q}}^*_{i+1})$; where $i = 1, \ldots, N_o$ represents the number of tested rotations. Let $\overline{\mathbf{q}}_i \overline{\mathbf{q}}^*_{i+1}$ be the true difference between two quaternions. The average quaternion $\overline{\mathbf{q}}$ can be found by maximizing $\overline{\mathbf{q}} = \arg\max \mathbf{q}^T \mathrm{M} \mathrm{q}$, where $\mathbf{M} \triangleq \sum_{j=1}^{N_s} \mathbf{q}_j \mathbf{q}_j^T$ and $j = 1, \ldots, N_s$ represents the number of samples. Thus, the average quaternion is retrieved as the eigenvector of $\mathbf{M}$ corresponding to the maximum eigenvalue [38].

Position precision, $Pre_{\mathbf{p}}$, for each location is simply defined as the standard deviation of measurements, $\mathrm{Pre}_p = \sqrt{(1/N_s)\sum_{j=1}^{N_s} \left\|\mathbf{p}_{\mathrm{ij}} - \overline{\mathbf{p}}_i\right\|^2}$. The same strategy is adopted for orientation precision, $\mathrm{Pre}_o = \sqrt{(1/N_s)\sum_{j=1}^{N_s} \left(2\cos^{-1}\left(\mathbf{q}_{\mathrm{ij}} \overline{\mathbf{q}}_i^*\right)\right)^2}$.

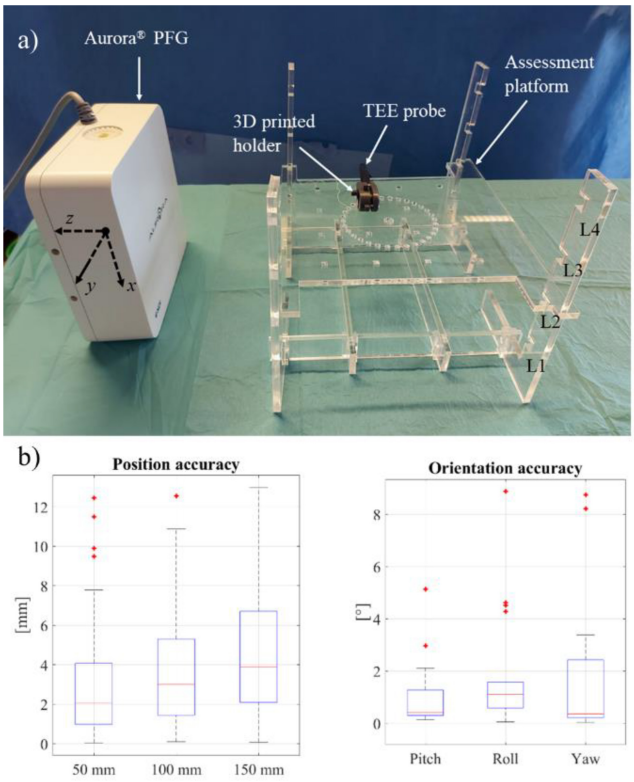

Fig. 5. Experimental results on the Hummel's board. (a) Experimental setup. (b) Position and orientation accuracies for different grid distances and rotation axes, respectively, in form of boxplots. Red stars represent outliers.

Assessment platform and numerical results on EM sensor errors using the Hummel's board are reported in form of boxplots (Fig. 5). The median position accuracies for 50, 100, 150 mm distance errors with the GE probe are 2.07, 2.99 and 3.88 mm respectively, thus the relative percentage error is always lower than 5%. The median position precision was 0.08 mm. The median orientation accuracy and precision are 0.41°(pitch), 1.11°(roll), 0.36°(yaw) and, 1.48° (pitch), 1.94° (roll), 1.43° (yaw), respectively.

B. Local-Global Registration

$\mathbf{R}^{\mathrm{IMU}}_{\mathrm{Coil}}$ and $\mathbf{R}^{\mathrm{Aurora}}_{\mathrm{ENU}}$ are estimated thanks to the extension of Chardonnen's method as reported in Section V-A. The registration error to evaluate the reliability of this strategy can be defined as the discrepancies between EM sensor orientation provided by Aurora, represented by $\mathbf{R}^{\mathrm{Aurora}}_{\mathrm{Coil}}$, and the IMU-based estimation, given by the following rotation matrices concatenation $\mathbf{R}^{\mathrm{Aurora}}_{\mathrm{ENU}} \mathbf{R}^{\mathrm{ENU}}_{\mathrm{IMU}} \mathbf{R}^{\mathrm{IMU}}_{\mathrm{Coil}}$.

The median registration errors on x, y and z Euler angles are: $-5.15°$, $-1.14°$ and 2.86°, respectively.

C. EKF-IKF Sensor Fusion

To evaluate the robustness of the sensor fusion finite state machine and angular velocity-based EM fault detection

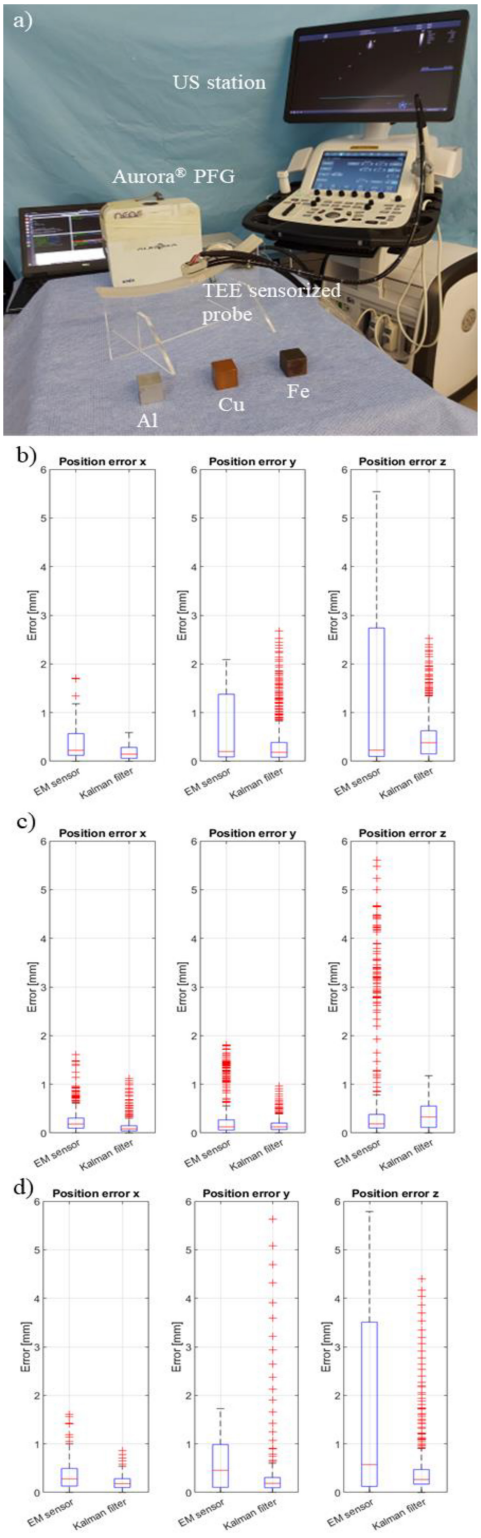

Fig. 6. Static results of the EKF-IKF-based finite state machine. In panel a) the experimental setup is shown, accounting of the TEE sensorized probe, US station, PFG and interfering cubes. Panels from b) to d) reports the tracking error boxplots on x, y and z of EM tracking VS sensor fusion for ferromagnetic (Fe cube), diamagnetic (Cu) and paramagnetic (Al) interferences, respectively. An indication on PFG reference frame is provided in Fig. 5.

approaches, three different cubes (30x30x30 mm^3 of iron, Fe, copper, Cu, and aluminum, Al) were positioned nearby the probe to mimic transient and steady state perturbations by different metallic objects. The three cubes were placed, one by one, between the sensorized probe, at known position (ground truth, GT) retrieved with an Aurora 6DOF probe, and PFG. This process was repeated three times for each cube in order to evaluate system repeatability. For these experiments, as there is no need to assess sensor fusion performances on all Hummel's board grid points and no standard protocol were found in literature, a 3D printed rail was considered. Raw EM data and sensor fusion output were compared with the GT to evaluate for system robustness and noise rejection. The experimental setup and results are reported in Fig. 6.

The proposed approach allows to significantly reduce the tracking error, especially on the z direction which is the most affected one by perturbances since is the only one along which interfering objects can be placed in between sensors and PFG (refer to Fig. 5 for an indication on the reference frame). Numerical results in the form of tracking error mean, median, standard deviation (σ) and interquartile range (IQ) are reported for x, y and z directions in Table I-III for the different interferences.

Last, statistical tests have been considered to objectively evaluate the finite state machine performances. A One-Sample Kolmogorov-Smirnov normality test was performed on the tracking errors after z-score normalization. It was observed that error distributions do not follow a normal distribution (p-value < 0.05). Additionally, a Mann-Whitney U-test demonstrated that the improvement of the sensor fusion strategy in position tracking with respect to standard EM sensors is statistically significant (p-value < 0.05) in all directions (x, y, z) and materials (aluminum, copper and iron cubes), with the exception of z direction with iron cube (p-value $= 0.8$).

D. FBGs for Temperature Estimation

The root-mean-square error (RMSE) between FBGs and the thermistor is calculated for each test run (FBGs free vs in the silicon). The first set of tests (FBGs free) shows an average RMSE of 1.59 °C, while the second set of tests (FBGs in silicone) shows an average RMSE of 4.35 °C. This increase in RMSE is due to the fact that the silicone shield affected the measurements when sudden temperature changes occurred. However, this feature does not affect the measurement of interest of gradual temperature fluctuations (see Fig. 7), which are the ones occurring during probe overheating for prolonged use in the esophagus.

VI. Conclusion & Future Outlook

This paper presents a novel multi-sensorization approach to improve safety during TEE-guided intracardiac interventions. These procedures are characterized by esophageal injuries for improperly placed and moved TEE probe and overheating.

To monitor TEE probe status over the procedure, we propose the use of sensors for position and temperature estimation. Specifically, sensor fusion between EM and IMU is developed for robust tracking, regardless of surrounding interferences, while FBGs is proposed for temperature sensing. A standardized assessment of EM performances for static

TABLE I
SENSOR FUSION RESULTS. NUMERIC VALUES FOR IRON PERTURBATION

Axis	Mean [mm]		Median [mm]		σ [mm]		IQ [mm]	
	EM	KF	EM	KF	EM	KF	EM	KF
x	0.35	0.17	0.23	0.14	0.31	0.12	1.70	0.58
y	0.61	0.38	0.19	0.18	0.67	0.51	2.08	2.67
z	1.42	0.49	0.23	0.38	1.93	0.47	5.54	2.52

TABLE II
SENSOR FUSION RESULTS. NUMERIC VALUES FOR COPPER PERTURBATION

Axis	Mean [mm]		Median [mm]		σ [mm]		IQ [mm]	
	EM	KF	EM	KF	EM	KF	EM	KF
x	0.27	0.19	0.19	0.12	0.24	0.20	1.61	1.11
y	0.53	0.13	0.17	0.10	0.56	0.13	1.80	0.96
z	1.19	0.38	0.23	0.35	1.45	0.28	5.61	1.17

TABLE III
SENSOR FUSION RESULTS. NUMERIC VALUES FOR ALUMINUM PERTURBATION

Axis	Mean [mm]		Median [mm]		σ [mm]		IQ [mm]	
	EM	KF	EM	KF	EM	KF	EM	KF
x	0.33	0.20	0.28	0.18	0.25	0.14	1.60	0.89
y	0.55	0.29	0.45	0.18	0.45	0.57	1.72	5.62
z	1.84	0.45	0.57	0.26	1.79	0.62	5.78	4.40

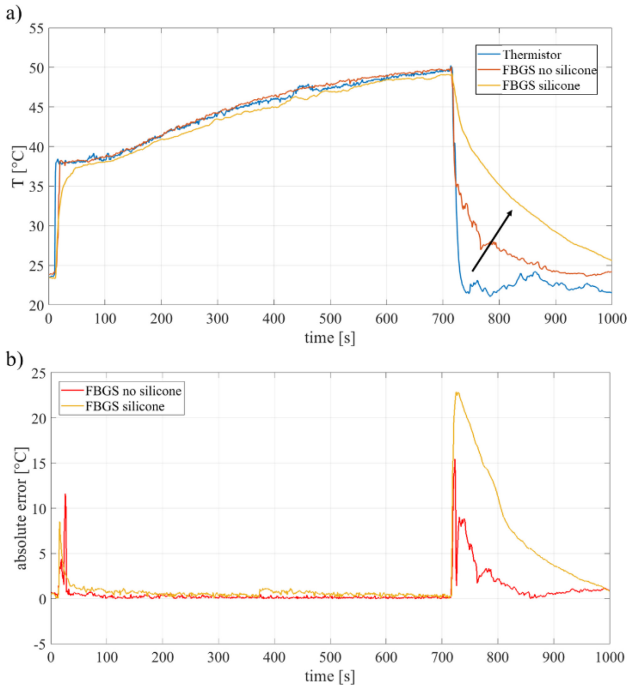

Fig. 7. Comparison of sensors performances for temperature estimation. In panel a) temperature profiles detected by thermistor, free FBGs and FBGs embedded in the silicone cuff are reported with different colors. The arrow highlights the increase in response time between the different configurations. Despite this, FBGs data closely match thermistor measurements during the slow heating phase, which is the most representative for TEE probe overheating. This is further highlighted in panel b) where the absolute error profiles between the two conditions against thermistor are reported. During the slow heating phase, the temperature estimation error tends to zero for both the considered scenarios.

TEE probe tracking is performed on the GE probe through Hummel's protocol. To the best of our knowledge, despite the extended use of these sensors for TEE probe tracking, a similar evaluation is still missing even though examining EM potentialities for the specific application is fundamental. Results on the 6VT-D TEE probe (GE Healthcare, Chicago, Illinois, USA) highlights position and orientation accuracies around 2 mm and 1°, respectively, which are comparable to values reported in literature on other ultrasound devices, as 2D and 4D hand-held probes [39], [40]. As these performances are expected to worsen when moving to the operating room, a finite state machine based on the combination of EKF and IKF is proposed to perform sensor fusion between EM and IMU, achieving a statistically significant improvement as confirmed by the Mann-Whitney U-test. Local Chardonnens' registration method is extended to global reference frames, with mean registration error of 3°. The limited performances, comparable with other state-of-the-art POA solutions [35], can be explained considering that IMU orientation is estimated with accelerometer and magnetometer data, which can be altered during acquisition by the magnetic field generated by the Aurora PFG (even after proper calibration). This issue was already reported in [35] where authors proposed to place IMU and EM sensors at least 3 cm apart one from the other to limit such distortions and improve registration performances. Anyway, in our application this is unfeasible since sensors should be placed on a small TEE probe tip. A novel EM sensor fault detection based on angular velocities is presented. This is advantageous with respect to magnetometer-based fault detection as it allows to be robust and sensitive to different interference sources, such as ferro- and paramagnetic materials. This approach is used to switch between EKF and IKF in a finite state machine-based fusion algorithm. Statistical tests, as the Mann-Whitney nonparametric U-test, demonstrated a consistent improvement of our method with respect to raw electromagnetic data in tracking performances. Only on the z direction for the iron cube disturbances the

proposed sensor fusion approach did not outperformed standard EM tracking. This is likely due to the fact that the z direction is the only one along which disturbances can be placed in between EM sensor and PFG (see Fig. 5a for a schematic on the Aurora reference frame) and that iron, being ferromagnetic, represents the greatest source of disturbances among the ones tested for the EM sensors. Anyway, the positive action of sensor fusion in reducing tracking error magnitude is evident from boxplots in Fig. 6b. Independently on the applied disturbance, the maximum tracking error is lower than 3.47 mm, as reported in [12], with the exception of few data points with the Al cube right before EM fault detection and IKF activation. The maximum tracking error with iron or copper disturbances is 2.67 mm (23% lower than the one reported in [12]). The outliers present with the Al cube occurs during the transition phases (i.e., when the cube is approaching or leaving the EM sensor). This is due to the fact the being Al paramagnetic it has lower interfering properties than Fe and Cu (ferro- and diamagnetic respectively) and thus the interference detection is less prompt allowing few of the first corrupted EM tracking points to be still considered valid. Last, FBGs-based temperature estimation is evaluated by comparing fiber performances with a commercial thermistor for biomedical applications. Tests based on sensors immersion in hot water reservoir with controlled temperature dynamics report a RMSE of 1.59 °C. This value increases up to 4.35 °C when embedding FBGs in the silicon cuff. However, this increment is mainly related to fast temperature changes and a lowered response time of the sensor. These rapid changes cannot be associated to probe overheating throughout the procedure, which is expected to be a slow phenomenon.

While these preliminary results provide insights on a multi-sensorization approach for TEE probe, several improvements are foreseen in the near future. We intend to extend the novel sensor fault detection and finite state machine EKF-IKF based sensor fusion also to dynamic scenarios, so to tackle all the procedural steps. Temperature estimation with FBGs should be exploited to develop automatic cooling system in order to avoid probe shutdown or retraction during delicate intracardiac catheter control. Last, the availability of sensor results in ROS will be exploited for integration in a robotic platform, enabling teleoperation or automatic control for probe manipulation.

Code Availability

The C++ and MATLAB codes used in this paper for the proposed generalized Chardonnens' registration and the finite state machine based on the integration of EKF and IKF are available at the following GitHub repository: https://github.com/giovanni-faoro/TEE-probe-sensorization.

Acknowledgment

The authors would like to thank Dr. Madhan Chirumamilla and Dr. Johan Vlekken for their support in the assessment of FBGs performances for temperature estimation.

References

[1] T. Doenst, M. Diab, C. Sponholz, M. Bauer, and G. Färber, "The opportunities and limitations of minimally invasive cardiac surgery," *Deutsches Arzteblatt Int.*, vol. 114, no. 46, pp. 777–784, Nov. 2017, doi: 10.3238/arztebl.2017.0777.

[2] A. P. W. Lee, Y. Y. Lam, G. W. K. Yip, R. M. Lang, Q. Zhang, and C. M. Yu, "Role of real time three-dimensional transesophageal echocardiography in guidance of interventional procedures in cardiology," *Heart*, vol. 96, no. 18, pp. 1485–1493, 2010, doi: 10.1136/hrt.2009.190025.

[3] R. T. Hahn et al., "Intraprocedural imaging of transcatheter tricuspid valve interventions," *JACC, Cardiovasc. Imag.*, vol. 12, no. 3, pp. 532–553, Mar. 2019, doi: 10.1016/j.jcmg.2018.07.034.

[4] A. B. Freitas-Ferraz et al., "Transesophageal echocardiography complications associated with interventional cardiology procedures," *Am. Heart J.*, vol. 221, pp. 19–28, Mar. 2020, doi: 10.1016/j.ahj.2019.11.018.

[5] A. B. Freitas-Ferraz et al., "Safety of transesophageal echocardiography to guide structural cardiac interventions," *J. Am. Coll. Cardiol.*, vol. 75, no. 25, pp. 3164–3173, Jun. 2020, doi: 10.1016/j.jacc.2020.04.069.

[6] A. Sorriento et al., "Optical and electromagnetic tracking systems for biomedical applications: A critical review on potentialities and limitations," *IEEE Rev. Biomed. Eng.*, vol. 13, pp. 212–232, 2020, doi: 10.1109/RBME.2019.2939091. [Online]. Available: https://ieeexplore.ieee.org/abstract/document/8822749?casa_token=VkwyCgFkJMEAAAAA:cWuCbbUOKpcprnxsOOhSBDWnyhzx_6jfdPmpemTJeRvIla8sRRaVxTR3n3gGM15PIQ4hoW2HfnK4

[7] A. M. Franz, T. Haidegger, W. Birkfellner, K. Cleary, T. M. Peters, and L. Maier-Hein, "Electromagnetic tracking in medicine—A review of technology, validation, and applications," *IEEE Trans Med. Imag.*, vol. 33, no. 8, pp. 1702–1725, Aug. 2014, doi: 10.1109/TMI.2014.2321777.

[8] J. B. Hummel et al., "Design and application of an assessment protocol for electromagnetic tracking systems," *Med. Phys.*, vol. 32, no. 7, pp. 2371–2379, 2005, doi: 10.1118/1.1944327.

[9] J. Hummel et al., "Evaluation of a new electromagnetic tracking system using a standardized assessment protocol," *Phys. Med. Biol.*, vol. 51, no. 10, p. N205, May 2006, doi: 10.1088/0031-9155/51/10/N01.

[10] E. Lugez, H. Sadjadi, D. R. Pichora, R. E. Ellis, S. G. Akl, and G. Fichtinger, "Electromagnetic tracking in surgical and interventional environments: usability study," *Int. J. Comput. Assist. Radiol. Surg.*, vol. 10, no. 3, pp. 253–262, Mar. 2015, doi: 10.1007/s11548-014-1110-0.

[11] H. Ren, D. Rank, M. Merdes, J. Stallkamp, and P. Kazanzides, "Multisensor data fusion in an integrated tracking system for endoscopic surgery," *IEEE Trans. Inf. Technol. Biomed.*, vol. 16, no. 1, pp. 106–111, Jan. 2012, doi: 10.1109/TITB.2011.2164088.

[12] Y. Zhang, K. Wang, J. Jiang, and Q. Tan, "Research on intraoperative organ motion tracking method based on fusion of inertial and electromagnetic navigation," *IEEE Access*, vol. 9, pp. 49069–49081, 2021, doi: 10.1109/ACCESS.2021.3068741.

[13] H. Sadjadi, K. Hashtrudi-Zaad, and G. Fichtinger, "Fusion of electromagnetic trackers to improve needle deflection estimation: Simulation study," *IEEE Trans. Biomed. Eng.*, vol. 60, no. 10, pp. 2706–2715, Oct. 2013, doi: 10.1109/TBME.2013.2262658.

[14] E. Lugez, H. Sadjadi, C. P. Joshi, K. Hashtrudi-Zaad, S. G. Akl, and G. Fichtinger, "Field distortion compensation for electromagnetic tracking of ultrasound probes with application in high-dose-rate prostate brachytherapy," *Biomed. Phys. Eng. Exp.*, vol. 5, no. 3, Apr. 2019, Art. no. 035026, doi: 10.1088/2057-1976/ab12b6.

[15] S. Navaei Lavasani, M. Deevband, P. Farnia, A. Ahmadian, and S. Saghatchi, "Compensation of dynamic electromagnetic field distortion using simultaneous localization and mapping method with application in endobronchial ultrasound-transbronchial needle aspiration (EBUS-TBNA) guidance," *Int. J. Med. Robot. Comput. Assist. Surg.*, vol. 16, no. 1, Feb. 2020, Art. no. e2035, doi: 10.1002/rcs.2035.

[16] C. R. Hatt, A. K. Jain, V. Parthasarathy, A. Lang, and A. N. Raval, "MRI-3D ultrasound-X-ray image fusion with electromagnetic tracking for transendocardial therapeutic injections: In-vitro validation and in-vivo feasibility," *Comput. Med. Imag. Graph.*, vol. 37, no. 2, pp. 162–173, Mar. 2013, doi: 10.1016/j.compmedimag.2013.03.006.

[17] R. Kreher et al., "A novel calibration phantom for combining echocardiography with electromagnetic tracking," *Curr. Direct. Biomed. Eng.*, vol. 6, no. 1, May 2020, Art. no. 20200003, doi: 10.1515/cdbme-2020-0003.

[18] M. Hastenteufel, M. Vetter, H. P. Meinzer, and I. Wolf, "Effect of 3D ultrasound probes on the accuracy of electromagnetic tracking systems," *Ultrasound Med. Biol.*, vol. 32, no. 9, pp. 1359–1368, Sep. 2006, doi: 10.1016/j.ultrasmedbio.2006.05.013.

[19] J. T. Moore et al., "Integration of trans-esophageal echocardiography with magnetic tracking technology for cardiac interventions," in *Proc. SPIE Med. Imag., Vis., Image-Guid. Proced., Model.*, 2010, pp. 930–939, doi: 10.1117/12.844273.

[20] J. T. Moore et al., "A navigation platform for guidance of beating heart transapical mitral valve repair," *IEEE Trans. Biomed. Eng.*, vol. 60, no. 4, pp. 1034–1040, Apr. 2013, doi: 10.1109/TBME.2012.2222405.

[21] S. Wang, D. Singh, D. Johnson, K. Althoefer, K. Rhode, and R. J. Housden, "Robotic ultrasound: View planning, tracking, and automatic acquisition of transesophageal echocardiography," *IEEE Robot. Autom. Mag.*, vol. 23, no. 4, pp. 118–127, Dec. 2016, doi: 10.1109/MRA.2016.2580478.

[22] S. Wang, X. Hou, J. Housden, Z. Hou, D. Singh, and K. Rhode, "IoT-based remote control study of a robotic trans-esophageal ultrasound probe via LAN and 5G," in *Medical Ultrasound, and Preterm, Perinatal and Paediatric Image Analysis* [Lecture Notes in Computer Science (Subseries of Lecture Notes in Artificial Intelligence and Lecture Notes in Bioinformatics)]. Cham, Switzerland: Springer, 2020, pp. 171–179, doi: 10.1007/978-3-030-60334-2_17.

[23] S. Wang et al., "Robotic intra-operative ultrasound: Virtual environments and parallel systems," *IEEE/CAA J. Automatica Sinica*, vol. 8, no. 5, pp. 1095–1106, May 2021, doi: 10.1109/JAS.2021.1003985.

[24] K. Li, Y. Xu, Z. Zhao, A. Li, and M. Q.-H. Meng, "Closed-loop magnetic manipulation for robotic transesophageal echocardiography," *IEEE Trans. Robot.*, vol. 39, no. 5, pp. 3946–3959, Oct. 2023, doi: 10.1109/TRO.2023.3281477.

[25] J. P. O'Shea et al., "Effects of prolonged transesophageal echocardiographic imaging and probe manipulation on the esophagus—An echocardiographic-pathologic study," *J. Am. Coll. Cardiol.*, vol. 17, no. 6, pp. 1426–1429, 1991, doi: 10.1016/S0735-1097(10)80158-5.

[26] "EPIQ 7 ultrasound system user manual release 1.0." 2013. [Online]. Available: www.healthcare.philips.com/ultrasound

[27] C. H. Stoner, A. B. Saunders, J. C. Heseltine, A. K. Cook, and J. A. Lidbury, "Prospective evaluation of complications associated with transesophageal echocardiography in dogs with congenital heart disease," *J Vet. Intern. Med.*, vol. 36, no. 2, pp. 406–416, Mar. 2022, doi: 10.1111/jvim.16356.

[28] D. A. McNamara et al., "Comparison of radiation exposure among interventional echocardiographers, interventional cardiologists, and sonographers during percutaneous structural heart interventions," *JAMA Netw. Open*, vol. 5, no. 7, Jul. 2022, Art. no. E2220597, doi: 10.1001/jamanetworkopen.2022.20597.

[29] C. Shi et al., "Shape sensing techniques for continuum robots in minimally invasive surgery: A survey," *IEEE Trans. Biomed. Eng.*, vol. 64, no. 8, pp. 1665–1678, Aug. 2017, doi: 10.1109/TBME.2016.2622361.

[30] R. Ben Hassen, A. Lemmers, and A. Delchambre, "Tri-axial force sensor in a soft catheter using fiber bragg gratings for endoscopic submucosal dissection," *IEEE Sens. J.*, vol. 23, no. 20, pp. 24626–24636, Oct. 2023, doi: 10.1109/JSEN.2023.3313172.

[31] P. Roriz, S. Silva, O. Frazão, and S. Novais, "Optical fiber temperature sensors and their biomedical applications," *Sensors*, vol. 20, no. 7, p. 2113, Apr. 2020, doi: 10.3390/s20072113.

[32] J. Chardonnens, J. Favre, and K. Aminian, "An effortless procedure to align the local frame of an inertial measurement unit to the local frame of another motion capture system," *J. Biomech.*, vol. 45, no. 13, pp. 2297–2300, Aug. 2012, doi: 10.1016/j.jbiomech.2012.06.009.

[33] F. Von Haxthausen, S. Böttger, D. Wulff, J. Hagenah, V. García-Vázquez, and S. Ipsen, "Medical robotics for ultrasound imaging: Current systems and future trends," *Med. Surg. Robot.*, vol. 2, pp. 55–71, Mar. 2021, doi: 10.1007/s43154-020-00037-y.

[34] M. Khodarahmi and V. Maihami, "A review on Kalman filter models," *Arch. Comput. Methods Eng.*, vol. 30, no. 1, pp. 727–747, Jan. 2023, doi: 10.1007/s11831-022-09815-7.

[35] H. Ren and P. Kazanzides, "A paired-orientation alignment problem in a hybrid tracking system for computer assisted surgery," *J. Intell. Robot. Syst., Theory Appl.*, vol. 63, no. 2, pp. 151–161, Aug. 2011, doi: 10.1007/s10846-010-9475-y.

[36] Z.-Q. Zhang, X.-L. Meng, and J.-K. Wu, "Quaternion-based Kalman filter with vector selection for accurate orientation tracking," *IEEE Trans. Instrum. Meas.*, vol. 61, no. 10, pp. 2817–2824, Oct. 2012, doi: 10.1109/TIM.2012.2196397.

[37] M. Wang, G. Yan and X. Sun, "A new incremental Kalman filter under poor observation condition," *2017 2nd Int. Conf. Robot. Autom. Eng. (ICRAE)*, Shanghai, China, 2017, pp. 469-472, doi: 10.1109/ICRAE.2017.8291432.

[38] F. L. Markley, Y. Cheng, J. L. Crassidis, and Y. Oshman, "Averaging quaternions," *J. Guidance, Control Dyn.*, vol. 30, no. 4, pp. 1193–1197, 2007.

[39] A. M. Franz et al., "Electromagnetic tracking for US-guided interventions: Standardized assessment of a new compact field generator," *Int. J. Comput. Assist. Radiol. Surg.*, vol. 7, no. 6, pp. 813–818, 2012, doi: 10.1007/s11548-012-0740-3.

[40] J. Gomes-Fonseca et al., "Technical note: Assessment of electromagnetic tracking systems in a surgical environment using ultrasonography and ureteroscopy instruments for percutaneous renal access," *Med. Phys.*, vol. 47, no. 1, pp. 19–26, Jan. 2020, doi: 10.1002/mp.13879.

Open Access funding provided by 'Scuola Superiore "S.Anna" di Studi Universitari e di Perfezionamento' within the CRUI CARE Agreement